Electromagnetic transition from the 4^+ to 2^+ resonance in ^{8}Be measured via the radiative capture in ^{4}He+^{4}He

V. M. Datar[1,2], D. R. Chakrabarty[1], Suresh Kumar[1,2], V. Nanal[3], S. Pastore[4], R. B. Wiringa[5],
S. P. Behera[1], A. Chatterjee[1], D. Jenkins[6], C. J. Lister[5], E. T. Mirgule[1], A. Mitra[1], R. G.
Pillay[3], K. Ramachandran[1], O. J. Roberts[6], P. C. Rout[1,2], A. Shrivastava[1], and P. Sugathan[7]

[1]*Nuclear Physics Division, Bhabha Atomic Research Centre, Mumbai 400 085, India*
[2]*Homi Bhabha National Institute, Anushaktinagar, Mumbai 400 094, India*
[3]*Tata Institute of Fundamental Research, Mumbai 400 005, India*
[4]*Department of Physics and Astronomy, University of South Carolina, Columbia, SC 29208, USA*
[5]*Physics Division, Argonne National Laboratory, Argonne, IL 60439, USA*
[6]*Department of Physics, University of York, Heslington, York, Y010 5DD, UK and*
[7]*Inter University Accelerator Centre, New Delhi-110064, India*
(Dated: May 7, 2013)

An earlier measurement on the 4^+ to 2^+ radiative transition in ^{8}Be provided the first electromagnetic signature of its dumbbell-like shape. However, the large uncertainty in the measured cross section does not allow a stringent test of nuclear structure models. The present paper reports a more elaborate and precise measurement for this transition, via the radiative capture in the ^{4}He+^{4}He reaction, improving the accuracy by about a factor of three. The *ab initio* calculations of the radiative transition strength with improved three-nucleon forces are also presented. The experimental results are compared with the predictions of the alpha cluster model and *ab initio* calculations.

The nucleus ^{8}Be is a classic example of the occurrence of alpha clustering [1] in nuclei. Its formation from two alpha particles provides an intermediate step in the synthesis of ^{12}C [2] from the fusion of three alpha particles inside the stars. The nucleus is also the stepping stone to understand alpha-clustering in heavier self-conjugate 4n nuclei. The dumbbell-shaped nucleus exhibits rotational states manifested as resonances in the alpha-alpha scattering system. The electromagnetic transition between the excited resonant states in ^{8}Be, with spin-parities of 4^+ and 2^+, was reported earlier [3] in order to provide a test for its alpha cluster structure. The measurements were made at two beam energies, on and off the 4^+ resonance, by detecting the transition gamma rays in coincidence with the two alpha particles arising from the decay of the 2^+ final state. However, the measured cross section (with an uncertainty of ∼33%) and the inferred reduced electromagnetic transition rate were not precise enough to provide a stringent test for various models like the cluster model [4] and *ab initio* quantum Monte Carlo model [5]. The uncertainty arose mainly due to the large background of 4.44 MeV gamma rays originating from the interaction of the incident beam with the window of the chamber holding the helium gas target. The present work, using essentially the same method, is aimed at a more accurate measurement and also at more beam energies straddling the 4^+ resonance. The essential aspects in this improved measurement are a better pixelisation of the alpha particle detectors, a more efficient and segmented gamma ray detector and a better shielding of the gamma rays from the beam-window interaction mentioned above.

The experiment was carried out using beams of ^{4}He from the BARC-TIFR Pelletron Linac Facility at TIFR,
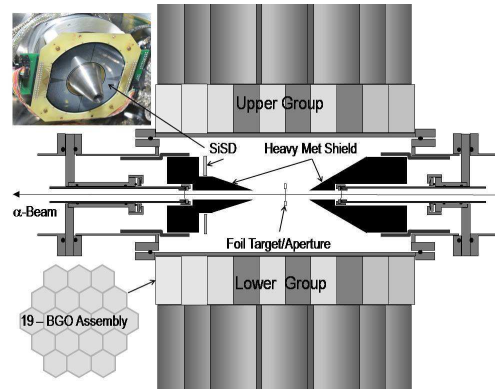

FIG. 1: (Color online) Schematic of experimental setup.

Mumbai at energies of $19-29$ MeV. The beam current was about 1 pnA on the target. The schematic of the experimental setup is shown in Fig. 1. The γ-rays were detected in a BGO detector array with a photopeak efficiency of about 23% at E_γ=8 MeV. The array consisted of 38 hexagonal cross section detectors, of length 76 mm and a face to face distance of 56 and 58 mm (in two groups), encased in thin aluminum housing. These were mounted in close packed groups of 19 each placed at ∼70 mm above and below the target. Alpha particles were detected in a 500 μm thick, annular, and double sided silicon strip detector (SiSD), with 2×16 θ rings (in left and right halves) and 16 ϕ sectors [6] with separate readouts. The active portion of the detector had an inner diameter of 48 mm and an outer diameter of 96 mm. The gap between the adjacent rings was 0.1 mm while that between adjacent sectors was 0.2 mm. The left and right halves of the θ
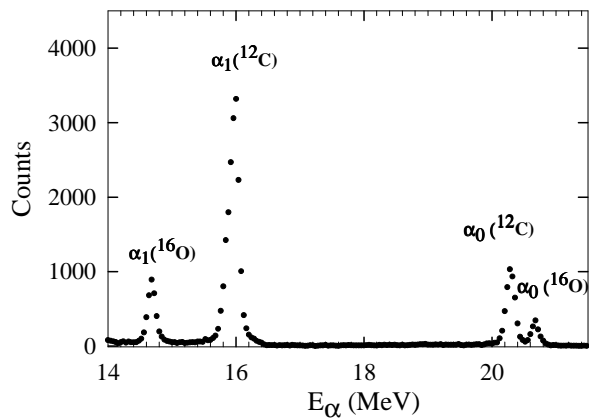
FIG. 2: Alpha particle spectra from the scattering on the mylar target at E_{beam}=22.4 MeV for a particular ring of the SiSD. Elastic and inelastic peaks (from the first excited states) from the ^{12}C and ^{16}O targets are indicated.

side were separated by 0.4 mm.

A chamber was designed to mount the strip detector at ∼70 mm from its centre in the forward direction and to hold the target helium gas (purity >99.9%) at ∼0.8 bar pressure. The gas was isolated from the beam line vacuum using ∼1 mg/cm^2 Kapton foils at the entry and the exit. The helium gas was filled using a gas handling setup similar to that used earlier [3]. Conical heavymet shields surrounded the Kapton windows in order to shield the BGO detector array from the copious 4.44 MeV γ-rays produced in the excitation of ^{12}C in the windows. The chamber had the provision to mount a ladder for holding a thick aluminum aperture plate with a hole of 24 mm diameter as well as thin mylar and carbon foils. The aperture plate, when placed at the centre of the target chamber, shielded the α-particles scattered from the Kapton entrance window and limited the effective beam-target interaction zone seen by the SiSD. The aperture diameter and the SiSD distance were decided on the basis of a Monte Carlo simulation [7] to get a reasonable efficiency for the detection of two α-particles following the radiative capture and subsequent decay of the final state in ^{8}Be. The typical effective target length was about 20 mm and the efficiency for the 2-α detection from the final state was about 35%, after including the effect of the various dead zones in the SiSD.

The energy and timing signals of the SiSD were generated from each of the 32 θ-rings (divided into two groups of the left and right halves) and 16 ϕ-sectors. The energy signals were sent to voltage sensitive analog-to-digital converters. Each timing signal was fanned out into two paths one being used to generate the overall particle event trigger for left rings, right rings and the sectors using a logical OR condition among the corresponding signals. In the other path the signals were fed to time to digital converters (TDCs) for measuring timing with respect to the γ-ray detector array. The anode signal from the photomultiplier of each of the 38 BGO detectors was

also fanned out for measuring the energy deposited by a charge-to-digital converter and for the timing measurement with respect to the SiSD using TDCs. A logical OR condition among the 38 signals produced the γ-ray event trigger. The grand event trigger was generated by requiring a fast coincidence between event triggers from the left and right halves of the SiSD θ-rings and that from the BGO-detector array. The data were collected in an event by event mode using a CAMAC based data acquisition (DAQ) system [8]. A 10 Hz pulser signal was fanned out and given to the test input of the three SiSD preamplifiers for estimating the dead time of the DAQ system.

The energy calibration of the SiSD detector was done using elastic and inelastic scattering of α-particles on ^{12}C and ^{16}O using thin carbon and mylar targets. A typical α-particle energy spectrum is shown in Fig. 2. The energy calibration was performed over the 256 (16×16) $\theta - \phi$ pixels. The 4.44 MeV and 6.13 MeV γ-rays from excited states in ^{12}C and ^{16}O populated through the inelastic α-particle scattering were used to calibrate the BGO detectors. These measurements were made periodically throughout the experiment in order to track the possible change in the calibrations of the α-particle and γ-ray detectors. A stability within ∼1% was witnessed over the period of the experiment.

The data were collected at four beam energies of 19.2, 22.4, 24.7, 28.9 MeV, spanning the 4^+ resonance in ^{8}Be, for the integrated beam charges of 81, 90, 125 and 58 pnC, respectively. The data was analyzed to extract the events corresponding to the γ-ray transition to the 2^+-final state in ^{8}Be and the subsequent 2-α decay of the final state. The first condition imposed was the prompt concidence among the γ-ray detector, at least one of the left rings and at least one of the right rings. This ensured a prompt coincidence also between the left and the right halves of the SiSD. The sector timing was also demanded to be in prompt coincidence with the γ-ray detector with two opposite sectors being simultaneously in coincidence. These conditions emphasized on the required events because the two α-particles from the decay of the final state are emitted at the azimuthal angles differing by ∼ 180°, neglecting the small momentum kick due to the transition γ-ray. Fig. 3 shows an example of the time spectrum between the BGO detector array and the SiSD at a beam energy of 22.4 MeV showing the prompt time peak. The hit-multiplicities of the left and the right rings were constrained to one for each and the energy deposited in the left and right halves (E_L and E_R) were constructed from the energy calibrations of the corresponding rings. For getting the γ-ray energy E_γ, the BGO detector with the highest γ-ray energy was taken to be the primary detector. The energies deposited in the neighbouring detectors, which were also in prompt coincidence and contained the leaked shower energy, were added to that of the primary detector for each event. An event by event reconstruction of the total α-particle energy, $E_{sum} = E_L + E_R$ was made with conditions of (a)
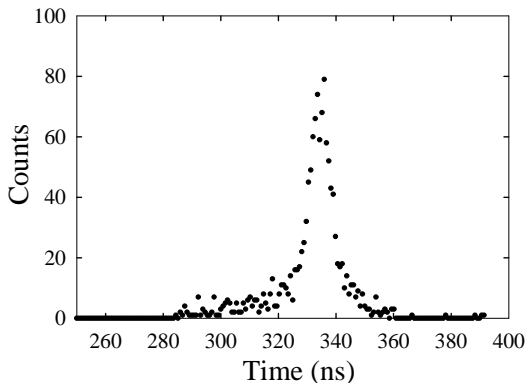
FIG. 3: Example of the time spectrum between the BGO detector array and the SiSD detector rings at E_{beam}=22.4 MeV.

FIG. 4: Two dimensional spectrum between E_{sum} =E_L+E_R (see text) and E_γ, generated with proper cuts as discussed in the text, at E_{beam}=22.4 MeV.

both E_L and E_R being within a lower and a upper limit ($\sim 1-13$ MeV) and (b) the reconstructed total energy and the total momentum of the two α-particles being within a proper two dimensional gate. These conditions were guided by the Monte Carlo simulations described below.

Fig.4 shows a two dimensional plot of E_{sum} vs E_γ at the beam energy of 22.4 MeV. A band of events around an E_{sum} of 13 MeV and E_γ of 8 MeV can be clearly identified. These events arise from the radiative capture of the two α-particles to the 2^+ resonance in ^{8}Be. A one dimensional spectrum of $E_{tot} = E_{sum} + E_\gamma$ is generated by putting one dimensional gates on E_{sum} of $8.8-15.0$ MeV and E_γ of $3.4-10.5$ MeV as suggested by simulation results. Similar E_{tot} spectra were generated at other beam energies by putting appropriate gates on these quantities. Fig.5 shows the E_{tot} spectra at all the four beam energies. The peaks in the spectra (not apparent at the highest beam energy which is beyond the extent of the 4^+-resonance), corresponding to the γ-ray transition between the resonances, were used in the calculation of the capture cross sections.

The extraction of radiative capture cross sections requires a simulation of the experimental set up using a Monte Carlo code. Such a simulation was done in two parts - one for the detection of the two α-particles and the other for the response of the BGO array to the incident γ-rays. The simulation for α-particle detection took into account the extended gas target, the aperture, the angular distribution of the α-particles emitted after the γ-decay and the geometry of the SiSD. The energy losses of the beam and decay α-particles, and the angular straggling, were calculated for each event using the SRIM code [9]. The inefficiencies of the SiSD due to gaps between rings and sectors were included. The γ-ray response was simulated using GEANT3 [10] with the angular distribution from the aligned 4^+ to the 2^+ final state included. For each event, the γ-ray energy was Doppler corrected. The simulated event by event data was written in a file for analysis by the same program that was used to sort the actual data. The simulated data were
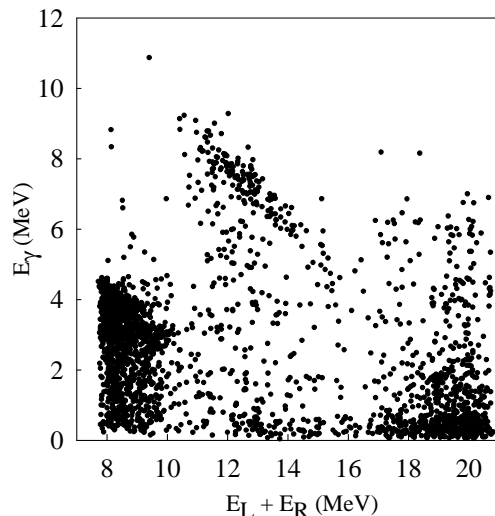
sorted to create the E_{tot} spectrum with the same conditions as used in the case of the actual data. Starting from the N_0 events corresponding to the 4^+ to 2^+ transition and the subsequent 2-α decay, the counts N in the same peak regions as shown in Fig.5 were calculated from the simulated spectra to get the overall detection efficiency (N/N_0) of the experimental set up. The simulation also provided the effective target thickness. The capture cross sections were extracted using the integrated beam charge, the target thickness and the detection efficiency. The effective α-particle energy $<E_\alpha>$ at each beam energy was also extracted from the simulation after knowing the interaction region and the energy loss of the incident beam in the entrance window and in the target gas up to the interaction region. The spread in the effective energy due to the finite extent of the interaction region was less than 0.14 MeV. The extracted cross sections at the four beam energies and the corresponding effective α-particle energies are tabulated in Table I.

TABLE I: Effective α-particle energies $<E_\alpha>$ and the radiative capture cross sections σ_γ extracted from the data at four beam energies (E_{beam}).

E_{beam} (MeV)	$<E_\alpha>$ (MeV)	σ_γ (nb)
19.2	18.44	102$\pm$12
22.4	21.80	149$\pm$16
24.7	24.08	131$\pm$13
28.9	28.40	<15

The extracted cross sections are plotted against the effective α-particle energies in Fig.6. The cross section at the resonance energy is consistent with the earlier measurement [3], but with an error of $\sim 10\%$ as compared to the earlier 33%. Fig.6 also shows the calculated cross
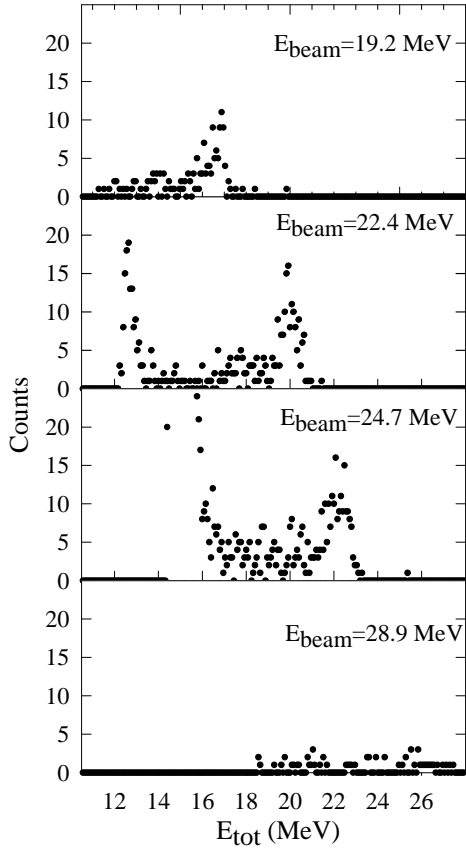
FIG. 5: One dimensional spectra of $E_{tot} = E_{sum} + E_\gamma$ generated with proper cuts at four beam energies.

FIG. 6: (Color online) Extracted capture cross sections plotted against the effective α-particle energy (see text). The last point indicates the upper bound of the cross section. The continuous line shows the result of a model calculation.

FIG. 7: (Color online) GFMC propagation with imaginary time τ of the (a) energy, (b) point proton radius, and (c) $E2$ matrix element; open stars denote the values extracted from the calculation.

sections from the cluster model calculation of [4]. The contribution from the partial waves of l=0, 2, 4 are added incoherently in this plot. The comparison with experimental data is good in the rising part of the cross section profile but deviates at higher energies. Whether a different choice of the $\alpha - \alpha$ potential along with a coherent summing over the various partial waves will improve the comparison remains to be seen. It may be mentioned that there is some ambiguity in the choice of the potentials giving similar values for the energies and widths of the resonant states of ^{8}Be.

Ab initio calculations of the radiative transition strengths in ^{8}Be, using realistic two- and three-nucleon interactions, were first reported in [5]. These variational Monte Carlo (VMC) calculations of the electric quadrupole moment Q and $B(E2)$ values indicated that the low-lying spectrum of ^{8}Be is well-described by the rotation of a common deformed two-α structure. Recently it has become possible to evaluate electroweak transitions with the more accurate Green's function Monte Carlo (GFMC) method [11], while improvements in the three-nucleon forces have also been made. We report here new GFMC calculations using the Argonne v_{18} (AV18) two-nucleon [12] and Illinois-7 (IL7) three-nucleon [13] potentials, which give a very nice reproduction of the energy spectrum and other properties of light nuclei in this mass
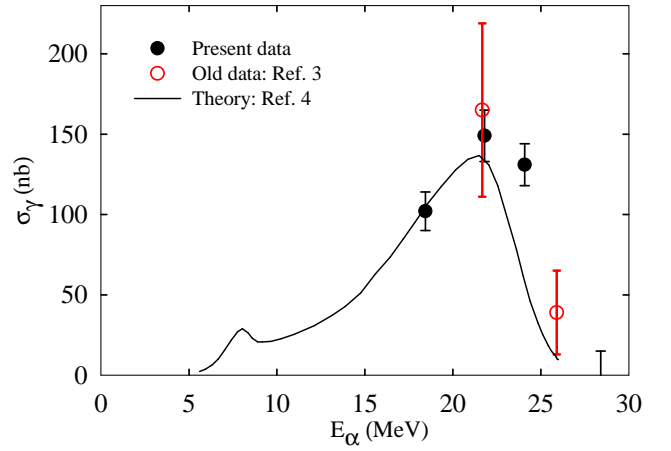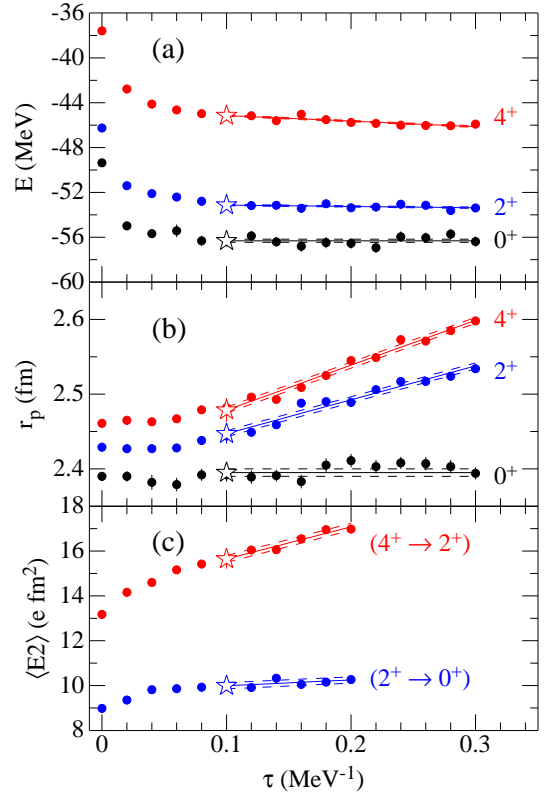
range [14].

An initial VMC calculation is made to generate a starting wave function, which the GFMC method then systematically improves upon by a propagation in imaginary time τ. The ^{8}Be 2$^+$ and 4$^+$ excited states are particularly

challenging because they tend to break up into two separate α-particles as τ increases. Figure 7 shows the propagation with imaginary time of the energies, radii, and $E2$ matrix elements. In Fig. 7(a), the energies of the states are seen to drop rapidly from the initial VMC energies at $\tau = 0$. The 0^+ ground state energy stabilizes and is well-fit by a constant averaged over $\tau = 0.1 - 0.3\,\mathrm{MeV}^{-1}$. The 2^+ state shows a very subtle decrease over the same range, while the 4^+ state drifts significantly lower; the energies quoted below are obtained from a linear fit using the value at $\tau = 0.1\,\mathrm{MeV}^{-1}$, with the Monte Carlo statistical error augmented by the range of values from $\tau = 0.08 - 0.12\,\mathrm{MeV}^{-1}$. This choice of τ should encompass the bulk of the improvement in the wave functions provided by the GFMC algorithm, before the tendency to dissolve into two α-particles sets in.

This tendency to dissolution is seen more strongly in the evolution of the point proton radii shown in Fig. 7(b). The 0^+ ground state radius is flat as a function of τ, while the 2^+ and 4^+ states both increase steadily from about $\tau = 0.1\,\mathrm{MeV}^{-1}$. The associated electric quadrupole moments, which are not shown, also increase steadily. Finally, the $E2$ matrix elements, shown in Fig. 7(c), also increase with τ, the effect being particularly pronounced with the $(4^+ \to 2^+)$ transition.

Results for the energies E, point proton radii r_p, electric quadrupole moments Q, and $B(E2)$ transition strengths are given in Table II. The absolute energies of the states are in excellent agreement with experiment. The quadrupole moments and $B(E2)$ values are consistent with an intrinsic quadrupole moment Q_0 of 32 ± 1 fm^2, which is about $\sim 20\%$ bigger than the original VMC calculation of [5].

TABLE II: GFMC results

J^π	E [MeV]	r_p [fm]	Q [fm^2]	$B(E2\downarrow)$
0^+	$-56.3(2)$	2.40	0	
2^+	$-53.1(1)$	2.45(1)	$-9.1(2)$	20.0(8)
4^+	$-45.1(2)$	2.48(2)	$-12.0(3)$	27.2(15)

A comparison with the *ab initio* calculation needs the present experimental result to be expressed in terms of the B(E2) value for the 4^+ to 2^+ transition. Whereas this is not straightforward, an approximate value can be calculated assuming a Breit Wigner form factor for the 4^+ resonance and using the experimental cross section at the resonance energy. This gives a partial gamma width $\Gamma_\gamma = (0.48\pm0.05)$ eV and a B(E2) value of $21\pm2.3\ e^2 fm^4$. This is somewhat lower than the calculated value. However, a better comparison will be possible after performing the *ab initio* calculation as a function of the alpha particle energy. The present experimental results, besides putting the α-cluster structure of ^{8}Be on a firmer footing, will provide data for testing the future calculations incorporating the reaction and the structure aspects in a seamless manner.

I. ACKNOWLEDGEMENT

[1] A. Bohr and B. R. Mottelson, Nuclear Structure, Vol. 2, Benjamin, New York (1975).
[2] F. Hoyle, Astrophys. J. Suppl. **1**, 121 (1954).
[3] V. M. Datar, Suresh Kumar, D. R. Chakrabarty, V. Nanal, E. T. Mirgule, A. Mitra, and H. H. Oza, Phys. Rev. Lett. **94**, 122502 (2005).
[4] K. Langanke and C. Rolfs, Zeit. Phys. **A324**, 307 (1986).
[5] R. B. Wiringa, S. C. Pieper, J. Carlson, and V. R. Pandharipande, Phys. Rev. C **62**, 014001 (2000).
[6] obtained from Micron Semiconductor Ltd., United Kingdom.
[7] V. M. Datar and Suresh Kumar, Proc. of Int. Symp. on Nucl. Phys. (Mumbai, 8-12 Dec. 2009) **54**, 704.
[8] A. Chatterjee, http://www.tifr.res.in/~pell/lamps
[9] J. F. Ziegler, http://www.srim.org
[10] GEANT, version 3.21, CERN program library.
[11] M. Pervin, S. C. Pieper, and R. B. Wiringa, Phys. Rev. C **76**, 064319 (2007).
[12] R. B. Wiringa, V. G. J. Stoks, and R. Schiavilla, Phys. Rev. C **51**, 38 (1995).
[13] Steven C. Pieper, AIP Conf. Proc. **1011**, 143 (2008).
[14] S. Pastore, S. C. Pieper, R. Schiavilla, and R. B. Wiringa, Phys. Rev. C **87**, 035503 (2013).